INTERLAMINAR FATIGUE GROWTH UNDER THERMAL CYCLES IN COMPOSITE LAMINATE

Toshio Nakamura*, Narayanan Ramanujam*, Pavankiran Vaddadi*, Raman P. Singh**
*** Department of Mechanical Engineering, SUNY at Stony Brook,**
****School of Mechanical and Aerospace Engineering, Oklahoma State University**

Keywords: *interlaminar fatigue crack, 3D FEM, mixed-mode fracture, energy release rate*

Abstract

A fatigue growth of fiber-reinforced composite laminate was characterized under a combined experimental and computational investigation. Here, 24-ply composites with pre-existing delamination were subjected to thermal cycles. During two month long test period, the crack growths were regularly monitored under variable amplitude. The measured data was used to determine the relationship between the temperature and growth rate. After completion of the test, inspections of fractured surfaces showed uneven growth with greater propagations near free surfaces. Due to such a behavior, 3D finite element analyses were performed to obtain energy release rate and mixed-mode stress intensity factors. The variations of these parameters were consistent with the observed crack front. The measured crack growth rates were also correlated with energy release rate to show good fit with the Paris law. The results are useful in understanding delamination growth under thermal cycles and estimating the threshold temperature to drive the growth.

1 Introduction

Fiber reinforced composites are commonly used as structural components in aerospace applications. In addition to designed mechanical or structural loads, they are often subjected to repeated temperature fluctuations during their service life. Since many composites are utilized in cross-ply arrangements, temperature changes can generate large internal thermal stresses. Typically, the difference in the coefficients of thermal expansion (CTE) along 0^o and 90^o directions exceeds $30\times10^{-6}/^oC$ which can produce thermal stresses of 20MPa or more under ΔT = 100°C. Furthermore, other environmental conditions such as moisture may also cause mismatch expansions and generate additional stresses within composite laminates. At smaller scale, hygrothermal stress stresses also arises from mismatch in properties between fibers and matrix [1]. These stresses arising from mismatch can generate matrix cracking that may also promote lamina delamination under thermal cycles.

Fatigue crack growth is one of major failure mechanisms in composites [2-4]. The fracture process of composite laminates subjected to fatigue loading involves a sequential accumulation of intralaminar and interlaminar damage in the form of transverse cracking, fiber splitting and delamination prior to catastrophic failure [5]. Fatigue of composite materials can be driven by mechanical loads, thermal loads or a combination of both [3]. Herakovich and Hyer [6] studied thermal cycling crack density as a function of layer thickness and number of transverse plies. Investigations on thermal delamination growth between laminae are rather limited. The effects of mechanical and thermal loads on fatigue were studied for curved layered composites [3]. The experimentally measured crack growth per unit temperature cycle was correlated to the difference in the energy release rate during thermal cycles [7].

2 Experimental Procedure

2.1 Specimen Preparation

The composite specimens were prepared from a prepreg tape with unidirectional carbon fibers (dia: 6-7μm) and Epon 862 epoxy are used. They are cured with Epikure 3234 in a vacuum bagging process. The specimen was cured at room temperature for 24 hours and post-cured for 2 hours at 120ºC. The laminate was fabricated with 12 0^o plies and 12 90^o plies with $[0^o_{12}/90^o_{12}]$ arrangement. This unique arrangement was chosen to maximize the thermal stress generated by the expansion mismatch between the cross plies. Prior to curing, a

pre-crack is introduced along this interface by inserting Teflon strips.

To determine properties of present composite lamina, separate 8-ply specimens with unidirectional fiber were fabricated using the same vacuum bagging process. Tensile tests were performed on these specimens to obtain load-displacement data as well as independent strain measurements from gages bonded on the specimen surface. The measured tensile moduli in the longitudinal and transverse directions were E_L = 105±2GPa and E_T = 5.5±0.08GPa, respectively. The estimated values of other relevant parameters for the transversely isotropic materials were ν_{LT} = 0.33, ν_{TT} = 0.30 and G_{LT} = 3.50GPa. The coefficients of thermal expansion (CTE) were determined using an environmental controlled chamber (Benchmaster BTRS). The longitudinal and transverse were estimated to be $\alpha_L = 0.63 \times 10^{-6}/^{o}C$ and $\alpha_T = 32 \times 10^{-6}/^{o}C$, respectively.

2.2 Thermal Cycles

The thermal cycle tests were conducted using the environmental chamber. In the current experiments, in order to isolate the effects of thermal cycles, the relative humidity was set at 0%. The objective of the thermal cycling tests was primarily two fold, first to measure length of crack growth as a function of the number of thermal cycles and second to observe the effect of temperature range on crack growth rate. Accordingly different ranges of temperatures were selected. A thermal cycle was carried out as follows. In the case of ΔT = 140°C, first, the temperature is maintained at 20°C for 10 minutes. This is followed by a steady ramp up to 160°C within 30 minutes. Then the temperature is held constant at 160°C for 30 minutes to ensure thermal equilibrium throughout the specimen.

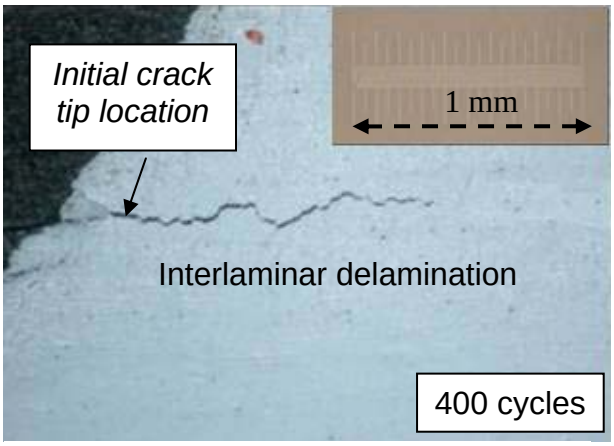

Fig. 1. Fatigue growth under thermal cycle.

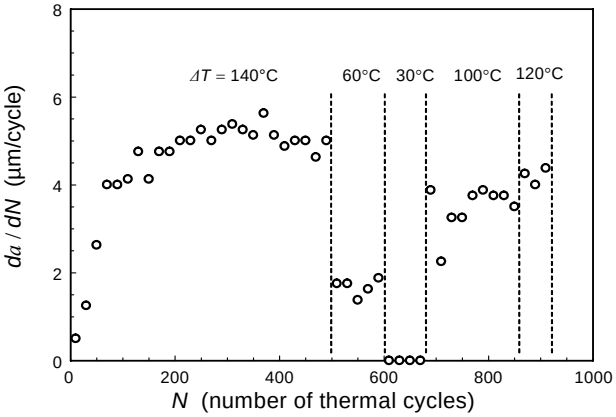

Fig. 2. Average growth rate under different of thermal cycles

Finally the specimen is cooled down to 20°C in 40 minutes. A single thermal cycle lasts about 110 minutes.

Crack length measurements were made after every twenty thermal cycles with simple visual crack detection after the specimen surfaces were masked by white correction tape to highlight the location of current crack tip. These measurements were made for two separate specimens under an optical microscope at a magnification of 50 times the original size. Two separate specimens were used in the measurement. For each specimen, the crack tip positions on both sides were measured. Figure 1 shows the optical micrographs of crack growths after different number of thermal cycles. For each measurement, a specimen is taken out of the environmental chamber for about 8 minutes which should be short enough to have minimal effects on the crack growth behavior. The rate of crack growth is shown as a function of thermal cycle in Fig. 2. Here the average of 4 measurements is plotted for up to 920 cycles or about 70 days. Note that these measurements were made at the surfaces and they do not represent the crack length through the thickness. The uneven growth will be discussed later. During the test, the temperature amplitudes were varied as indicated in the figure. Except for the initial amplitude of ΔT = 140°C where the large value was intentionally chosen to initiate the crack growth, the remaining amplitudes were arbitrary chosen. Total of five different amplitudes of ΔT = 140°C, 60°C, 30°C, 100°C, 120°C were prescribed during the measurement period.

At initial phase, it took about 240 cycles to reach steady state propagation under ΔT = 140°C condition. During the steady state, the growth rate was estimated to be da/dN = 5.1μm/cycle. At 500th cycle, the temperature amplitude was switched to

60°C and maintained for 100 cycles. The smaller number of cycles were chosen since it appeared that the propagation have reached the steady state much faster but at slower rate of about da/dN = 1.7μm/cycle. In the subsequent phase (after 600 cycles), ΔT was reduced to 30°C. Even after 80 cycles, the measurements showed no visible change in the crack length. It is likely that driving force to fatigue crack is below the threshold value. Note that prior to testing, we had no knowledge of rate of delamination growth for a given ΔT, and the temperature change had to be assigned based on the behavior of previous data. The next ΔT was chosen to be 100°C. As the measurements were made, it took longer time to reach the steady state. It is likely because the crack was arrested for about 6 days at T = 50°C and some healing might have occurred near the crack tip. To secure the steady state condition, ΔT = 100°C condition was kept for 180 cycles. For the final test, the temperature amplitude was set at ΔT = 120°C for 60 cycles.

2.3 Fracture Surfaces

After the thermal cycling test was completed, the fracture surfaces were carefully examined. First the specimens were placed in nitrogen bath to preserve surface conditions and they were split in half along the crack plane. Figure 3 shows an optical and SEM micrographs of the fracture surfaces which revealed unexpected crack growth phenomena. They show the propagation to be non-uniform across the thickness or crack front and crack growths appear to be initiated at the two edges. Near the mid-section, there was essentially no propagation. The propagation behavior is close to symmetric about the centerline and its average angle with respect to the initial crack front is measured to be 43.5°.
Closer inspection on the fractured surfaces shown in

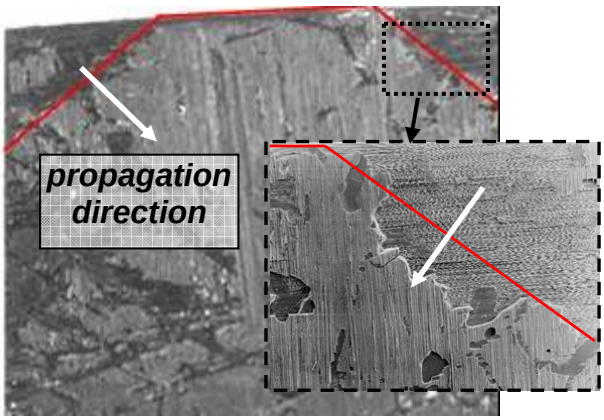

Fig. 3. Fractured surface showing angled front.

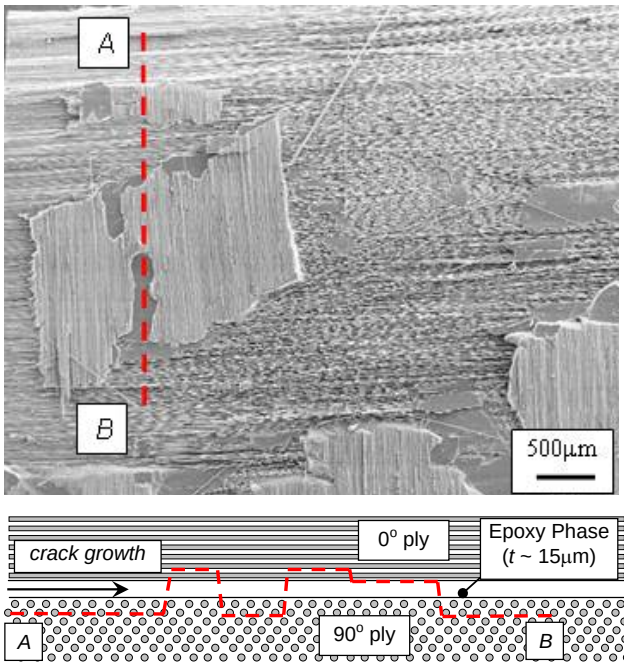

Fig. 4. Crack profile showing alternating path.

Fig. 4 also revealed alternating crack paths. As indicated, three difference surfaces were exposed; 0o fibers, 90° fibers and planar epoxy phase. It appears the crack alternated among these three regions as it propagated. The likely cause of this trend is that higher fracture toughness of interlaminar epoxy phase which was used to bond 0° and 90° plies. Also T-stress and mode II stress intensity factor KII might have played roles. Estimated crack path between *A* and *B* is also shown. Here the crack initiates 90° plies (near *A*) but switched to 0o ply. Afterward it continued to alternate its path as illustrated in the figure. Although not shown here, SEM micrograph of the other crack surface was also used to confirm the path. The total crack propagation at along the edges was about 6mm.

The inspection of fracture surfaces dictates the necessity to carry our 3D fracture analysis. The following section describes the computational procedure used to determine the energy release rate as well as mixed-mode stress intensity factors.

3 Computational Analysis of 3D Thermal Crack

3.1 Finite Element Models

Since no analytical solutions exist for the 3D crack front in the composite laminate, finite element model was constructed to identify the relationship between thermal load and the fracture parameters. Here several crack front configurations were considered starting with the initial straight crack

front to the final angled or kinked crack front shown in Fig. 3. To construct the crack front configuration, dimensions of fracture surfaces of two specimens were carefully measured. As described in the previous section, the crack front consists of three nearly linear sections. One at the middles and two inclined at the sides with the kink angle being 43.5°. Since intermediate crack front shapes were not known, we assumed them to maintain the similar angle between the middle crack front and the angled crack front. Although other growth models are possible, all should have similar fracture parameter variations (e.g., energy release rate along crack front), at least qualitatively. In this study, three separate models representing different stages of crack growth were constructed as shown in Fig. 5. The first model (crack front *A*) is for the initial stage possessing a straight crack front along the width direction (the configuration prior to thermal cycling). Next model corresponds to an intermediate stage of crack propagation (crack front *B*) with growth at edge being Δa_{edge} = 2.93mm. A third model (crack front *C*) represents the measured growth at the final stage with Δa_{edge} = 5.85mm. In addition, the crack growth was assumed to be planar although the (vertically) alternating crack paths were observed as shown in Fig. 4.

In order to construct the finite element model, a mesh generator was developed. In order to ensure accurate computations of mixed-mode stress

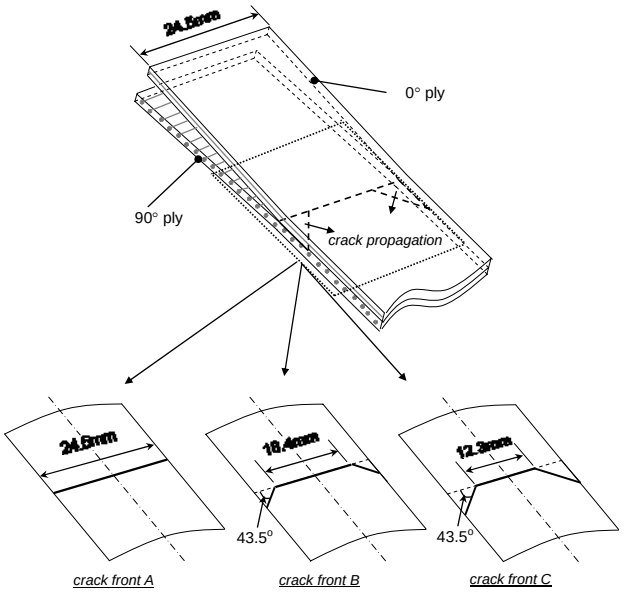

Fig. 5. Schematics of composite model, and three different crack configurations analyzed. Initial stage (crack front *A*), Intermediate stage (crack front *B*) and final stage (crack front *C*).

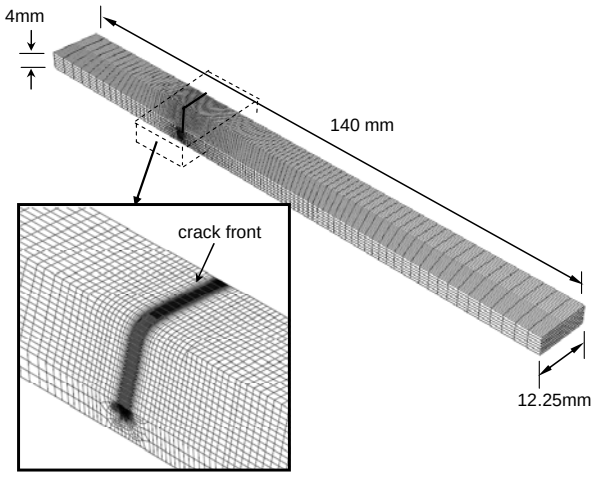

Fig. 6. 3D Finite element mesh for crank front C model. A enlarge section of 90° exposing the crack front region is also shown.

intensity factors along the crack front, a special care was taken in the mesh design. First the symmetry condition was utilized to model only a half of the actual specimens. Second fine elements are focused at the crack front and 30 element layers were taken along the half-width of the specimen. The final crack growth configuration model shown in Fig. 6 contains approximately 60,000 eight noded brick elements. The material model was chosen to be transversely isotropic and the properties reported in section 2.2 were assigned. Here, the upper half was modeled as 0o lamina (fibers in the direction of crack growth) while the bottom half is modeled as 90o lamina (fibers perpendicular to the direction of crack growth). During trial computations, a limited overlapping of top and bottom crack surfaces was observed (due to large Mode II condition). In order to circumvent the problem, contact conditions are enforced between the fracture faces to have physically consistent model. Furthermore, in order to minimize calculation errors for fracture parameters, the angled crack location was slightly smoothed by introducing a narrow transition region (1.7mm wide).

3.2 Computed Fracture Parameters

Since the material is linear elastic, a single computation is necessary for relating fracture parameters to the temperature change in each crack model. The loading was imposed by assigned an increased temperature throughout the model. The energy release rates as well as the mixed mode stress intensity factors were computed at nodal points along the crack front. The energy release rates for three models are shown as a function of the arc length of the crack front in Fig. 7. Here the energy

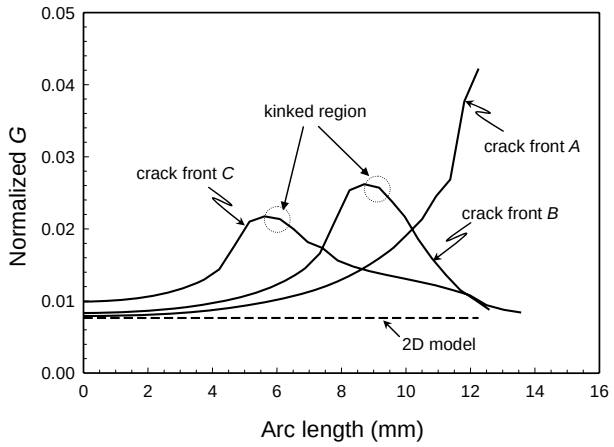

Fig. 7. Point-wise energy release rate values along the crack front at various stages of fatigue growth during thermal cycling.

release rate is normalized with $hE_L(\Delta\alpha\Delta T)^2$, where h is the laminate thickness (4mm) and $\Delta\alpha = \alpha_T - \alpha_L$. The energy release rate variation for the crack front A shows a steep raise near the edge. In fact, the local G near the edge is about 5 times as large as the local G near the mid-span. Such a behavior is consistent with 3D interface crack under dominant Mode II condition [8]. Furthermore it support that the initiation point of crack growth to be at the edge as suggested by the fracture surfaces. For the other two models, the angled or kinked region is indicated in the figure. In each case, the maximum G is close to this region and local G decreases toward the edge beyond this point. This indicates the crack to also grow inward from the edge toward the mid-point with shifting of kink point. In addition, the energy release rate is more even across the crack front in these models. In fact the difference between the minimum and maximum G is only about 2 times for crack front C model. no analytical solutions exist for the 3D crack front in the composite laminate, finite element

Due to the nature of thermal loading, primary mode of crack growth was under Mode II. In order to quantify the mixed-mode states, the phase angles for the 3D interface crack are determined. The phase angle was obtained through stresses as

$$\psi(L) = \tan^{-1}\left[\left(\frac{\sigma_{12}}{\eta\sigma_{22}}\right)_{r=L}\right] \qquad (1)$$

Here, L is the characteristic length scale which is chosen as 80 μm and η is the traction resolution factor. In order to study the relative strength of each mode in 3D crack front, apart from the phase angle

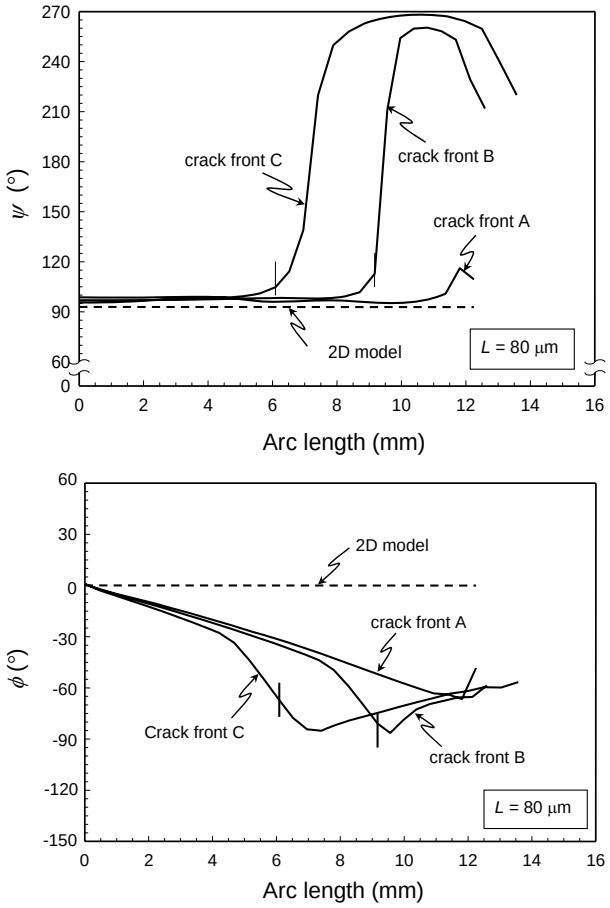

Fig. 8. Comparison between variation of phase angles along crack fronts of three different models.

ψ that describes relative strength of in-plane deformation there is an additional phase angle ϕ that describes relative strength of anti-plane deformation. This can be defined as

$$\phi = \tan^{-1}\left(\frac{\sigma_{23}}{\sqrt{\sigma_{12}^{\ 2} + \sigma_{22}^{\ 2} + \sigma_{23}^{\ 2}}}\right) \qquad (2)$$

Results of both phase angles are shown in Fig. 8. The in-plane mode shows large Mode II with respect to Mode I along straight crack front for all cases. Near the kink region, there are more Mode I but Mode II dominates along the angled front. The anti-plane shear mode is zero at the mid-point but it gradually increases in amplitude toward the edge. The relative value of Mode II appears to be largest near the kink region.

4 Fatigue Crack Growth

Like homogeneous materials, threshold resistances of fatigue growth for composites are

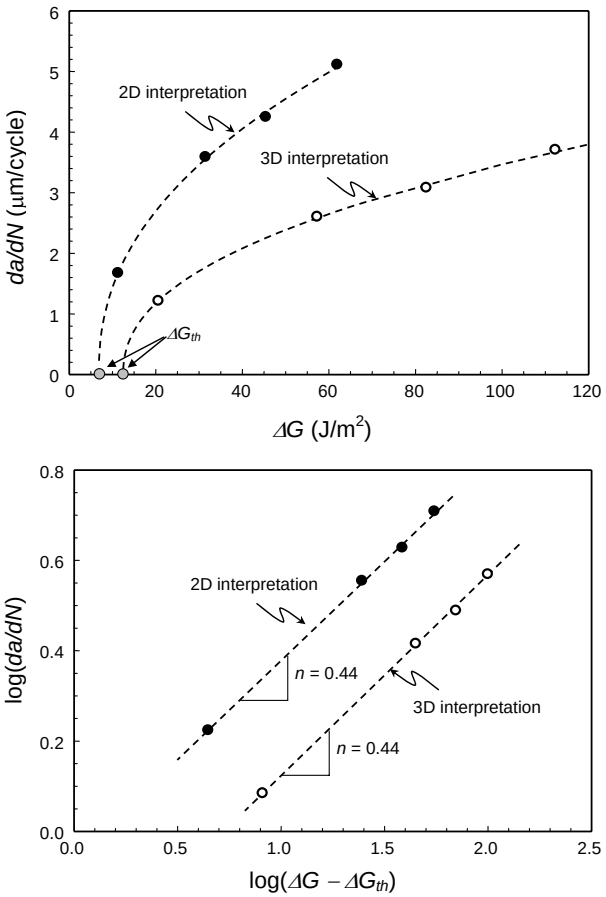

Fig. 9. Fatigue crack growth rates with corresponding energy release rates ΔG based on 3D and 2D interpretations including power law fit and on log-log plot.

expected to be less that that under monotonic loading. Here we inspect the fatigue crack growth rate (da/dN) to determine the remaining life or an inspection interval of component. Here based on the observed crack growths during thermal cycles and the relationship between the energy release rate and temperature change, rate of fatigue growth is characterized. Since the local G is not uniform over the inclined or growing portion of the crack front, the average value was chosen from the results of crack front C model shown in Fig. 9. It is $G_{ave}/hE_L(\Delta\alpha\Delta T)^2$ = 0.0139. Also since the actual crack growth is directed towards inward as well, the true growth rate is determined by multiplying the observed crack growth at edges by cos43.5°. The results are listed in Table 2. In order to gauge the three-dimensional effects, a separate 2D model was constructed and *apparent* energy release rate and growth rate are also listed in the same table. The 2D model assumes plane strain condition and its relationship between G and ΔT was computed as $G_{2D}/hE_L(\Delta\alpha\Delta T)^2$ = 0.0.76. Since 3D crack growth shape is not possible to determine in actual laminate, this apparent relation based on 2D interpretation should be useful in evaluating thermal fatigue growth. Both results are plotted in Fig. 9.

Since a power law equation based on Paris law [9] is a most common approach to relation the crack driving force and the growth rate, the following formula is considered.

$$\frac{da}{dN} = C\left(\Delta G - \Delta G_{th}\right)^n \qquad (3)$$

Here C and n are the material constants, and ΔG_{th} is the threshold fatigue toughness. Using the curve fitting program, The following values were obtained for 3D interpretations, C = 0.482×10^{-6} [m/cycle(J/m^2)^n], n = 0.44 and ΔG_{th} = 12.5J/m^2. For 2D interpretation, they were C = 0.869×10^{-6} [m/cycle(J/m^2)^n], n = 0.44 and ΔG_{th} = 6.9/m^2. These curves are also drawn in Fig. 11(a), which shows very good much. Note this fatigue law does not into effects of mixed-mode. However, since the mode-mixity is nearly constant through crack growth as shown in the results of crack front A, B, C, these parameters should be valid for dominantly Mode II condition. In general, toughness is higher under dominant Mode II. The results are also shown in log-log scale plot in Fig. 11(b). It also confirms good matches with the power law equation. These results also show lesser ΔG_{th} and higher fatigue growth rate according to 2D interpretations. A similar power law equation is possible with the stress intensity. Note the exponent would be double in those cases.

5 Discussions

With typical cross-ply arrangements, each lamina is more constrained and crack growth under thermal condition is probably more difficult than the current specimen configurations. However if they are subjected to combined cyclic mechanical and thermal loads, the likelihood of fatigue crack growth increases. Here a detailed investigation has been conducted to study the thermal cycle driven fatigue crack propagation along the cross-ply interface.

In the current study, laminates were fabricated using vacuum bagging technique that enabled introduction of pre-existing delamination. In practice, delamination may occur due to weak bonding or after repeated mechanical loading and/or under severe environmental conditions. The present tests confirmed such crack can growth under thermal

cycles albeit with certain conditions. Examination of the fractured surface at the conclusion of experiment revealed complex crack propagation pattern. Interpretations for an uneven crack growth from an initially straight front can be made with recourse to 3D interpretation. First the local/point-wise energy release rate value and the two phase angles have been computed along the three-dimensional crack front. Next, the crack growth rate has been correlated with range of energy release rate using a power law relation. Furthermore, a threshold value of range of energy release rate (ΔG_{th}) has been estimated below which there is no crack propagation. Computations show that values for energy release rate are higher for the three-dimensional case compared to the two-dimensional case for similar thermal loading conditions. Thus 2D interpretation would offer a conservative estimate for fatigue life of cross-ply laminates submitted to thermal cycling. While many studies on carbon fiber reinforced epoxy laminates might base their studies on two-dimensional computational analyses for fatigue crack growth characterization, our study reveals that three-dimensional effects play a significant role on the interface crack propagation behavior in laminated composites.

Reported values of interlaminar toughness ranges G_c = 300 – 1,000J/m^2 [10] while the estimated value of threshold fatigue crack growth was only ΔG_{th} = 12.5J/m^2. This shows under thermal cycles, much smaller load is necessary to propagate the existing crack. In fact, the corresponding temperature for threshold is only ΔT = 47^{o}C. The present study underlines the procedure for careful observation through experiments followed by a suitable computational analysis for fatigue crack characterization. Future studies undertaken could involve examination of crack propagation pattern evolution for different laminate lay-ups and operating conditions including hygrothermal fatigue.

References

[1] Vaddadi P, Nakamura T. and Singh R. “Transient hygrothermal stresses in fiber reinforced composites: a heterogeneous characterization approach”. *Composites Part A: Applied Science and Manufacturing,* Vol. 34, No. 8, pp 719-730, 2003.

[2] Lowe A, Kwon O.H. and Mai, Y.W. “Fatigue and fracture behavior of novel rubber modified epoxy resins”. *Polymer*, Vol. 37, No. 4, pp 565-572, 1996.

[3] Figiel L. and Kaminski M. “Mechanical and thermal fatigue delamination of curved layered composites”. *Computers and Structures,* Vol. 81, No. 18-19, pp 1865-1873, 2003.

[4] Lafarie-Frenot M.C. and Ho N.Q. “Influence of free edge intralaminar stresses on damage process in CFRP laminates under thermal cycling conditions”. *Composites Science and Technology,* Vol. 66, No. 10, pp 1354-1365, 2006.

[5] Kashtalyan M. and Soutis C. “Analysis of composite laminates with intra- and interlaminar damage”. *Progress in Aerospace Sciences,* Vol. 41, No. 2, pp 152-173, 2005.

[6] Herakovich C.T. and Hyer M.W. “Damage-induced property changes in composites subjected to cyclic thermal loading”. *Engineering Fracture Mechanics,* Vol. 25, No. 5-6, pp 779-791, 1986.

[7] Gurumurthy C.K., Kramer E.J. and Hui C.Y. “Hydro-thermal fatigue of polymer interfaces”. *Acta Materialia,* Vol. 49, No. 16, pp 3309-3320, 2001.

[8] Nakamura T. and Parks, D.M. “Anti-symmetrical 3D stress field near the crack front of a thin elastic plate. *International Journal of Solids and Structures* , Vol. 25, pp 1411-1426, 1989.

[9] Paris P.C., Gomez M.P. and Anderson W.E. “A rational analytic theory of fatigue”. *The Trend in Engineering,* Vol. 13, No. 1, pp 9-14, 1961

[10] Grady J.E. and Sun C.T. “Dynamic delamination crack propagation in graphite/epoxy laminate”. *ASTM STP*, Vol. 907, pp 5-31, 1986.